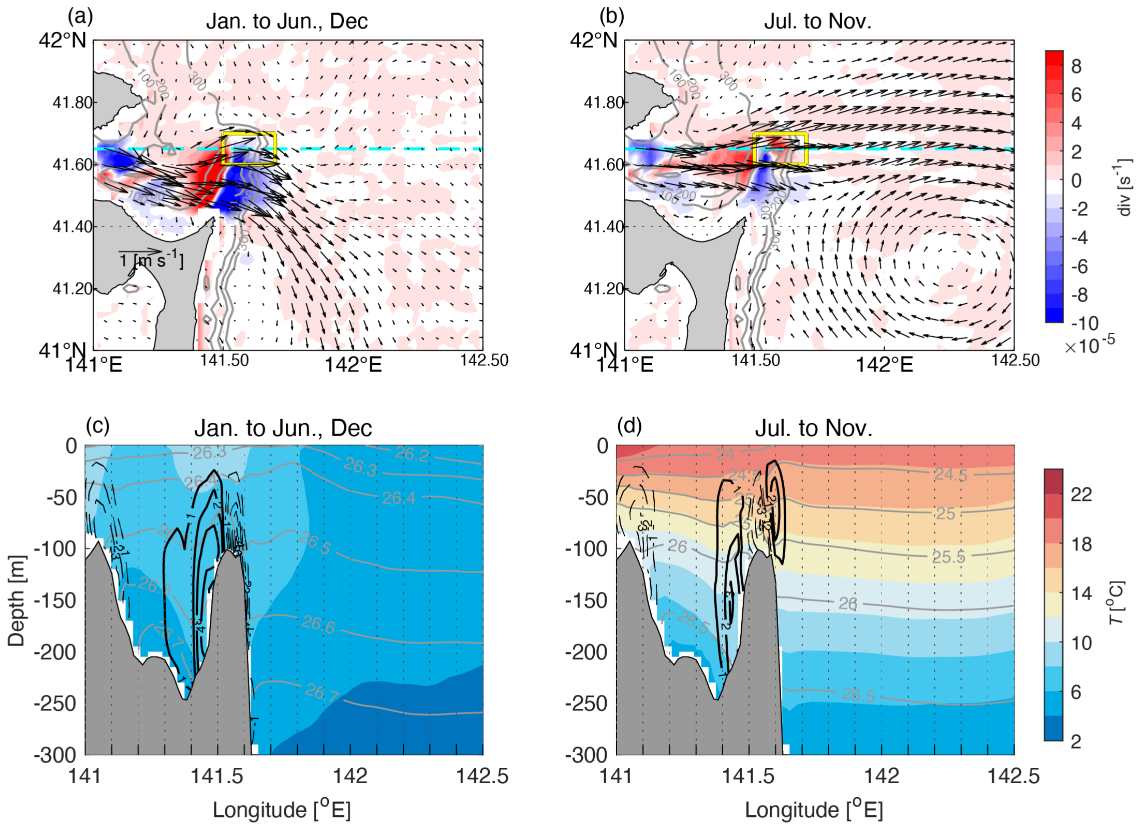

Supplementary Fig. 1 | Seasonal variability characteristics of the Tsugaru Warm Current on the basis of the JCOPE-T DA 2019 output. Upper panel: The mean surface horizontal current velocities and their divergence (positive) and convergence (negative) (**a**, December, January–June and **b**, July–November averages). The grey contours in **a** and **b** indicate the water depth. The dashed cyan line in **a** and **b** indicates the latitude of the vertical cross sections shown in **c** and **d**. The yellow rectangles in **a** and **b** indicate the area of 41.6°N–41.7°N, 141.5°E–141.7°E (see main text). Bottom panel: east–west vertical section along 41.65°N (**c**, December, January–June; **d**, July–November mean). The colours in **c** and **d** indicate the water temperature, the grey contours indicate the potential density anomaly, and the black contours represent the vertical velocity (the solid lines represent upwelling, and the dashed lines represent downwelling). Source data are provided as a Source Data file.

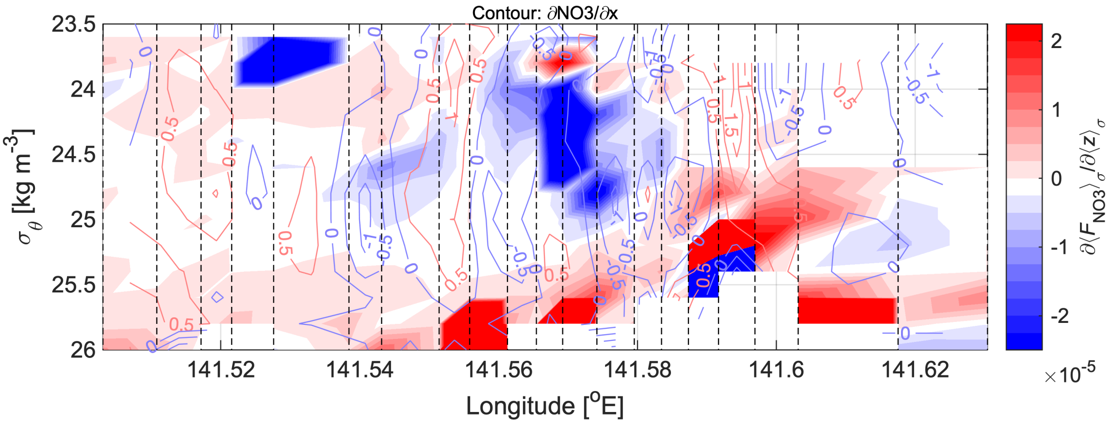

Supplementary Fig. 2 | Vertical nitrate flux convergence (depicted by colour shading; warm colours denote convergence) and the east–west gradient of nitrate (depicted by contours) in isopycnal surface coordinates along the drift observation. The isopycnal mean flux ($\langle F_{NO3}\rangle_\sigma$) and depth ($\langle z\rangle_\sigma$; upward negative) for convergence calculations are computed at intervals of 0.2 σ_θ. The density for the zonal gradient calculations is also determined every 0.2 σ_θ. The colour of the contours indicates the sign (blue: negative; red: positive). The vertical dashed line marks the location of the observation point.

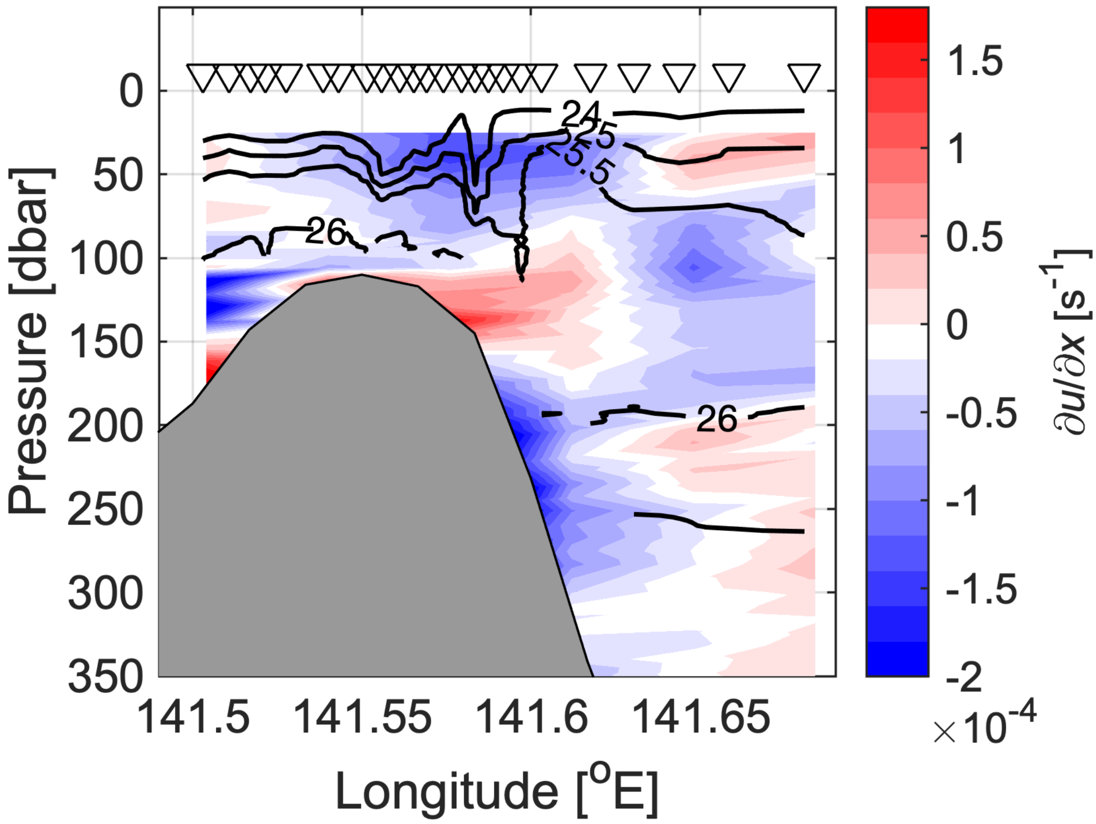

Supplementary Fig. 3 | Zonal velocity divergence along the drift observation obtained from an acoustic Doppler current profiler mounted on the R/V Wakataka-Maru (SADCP). The thick black contours denote potential density anomalies. The triangles indicate the deployment longitude of the microstructure profiler (Turbulence Ocean Microstructure Acquisition Profiler; TurboMAP) during the drift observation. Source data are provided as a Source Data file.

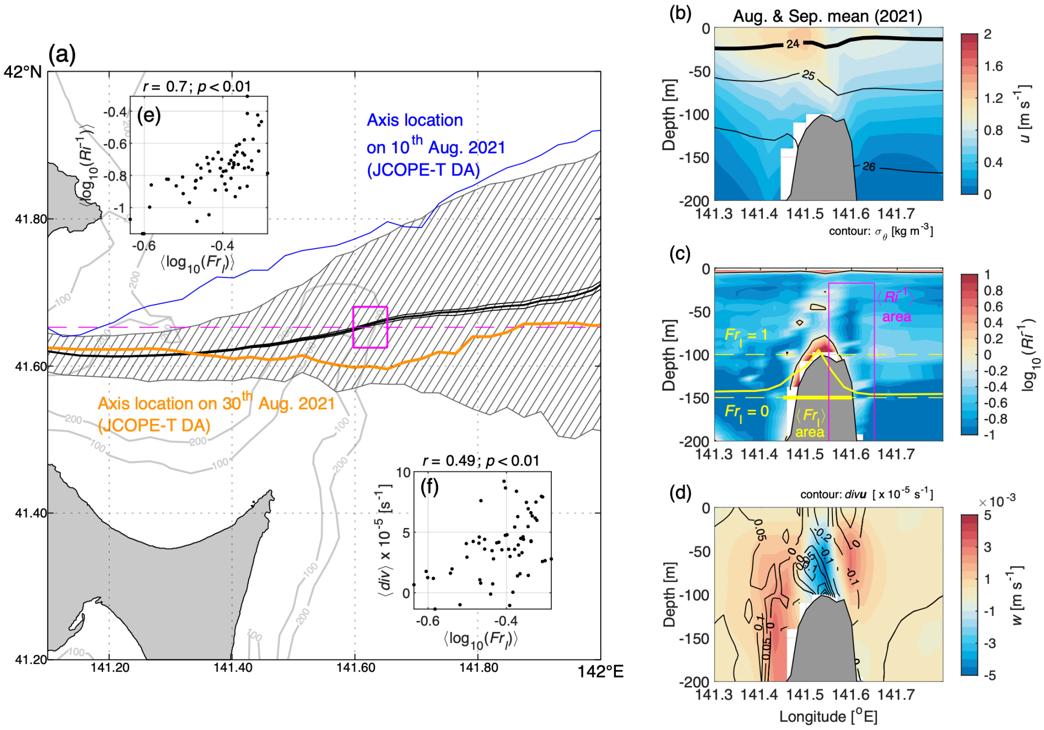

Supplementary Fig. 4 | Interaction between the intense current and the sill suggested by JCOPE-T DA. a, Distribution of the Tsugaru Warm Current axis positions obtained from the JCOPE-T DA 2021 August and September outputs. Hatching represents the 95% percentile in latitude for the duration. The black bold line and black thin lines represent the bootstrapped mean and the bootstrapped 95% confidence interval of the mean, respectively. The magenta dashed line indicates the latitude of the vertical sections in **b**–**d**; the magenta rectangle indicates the mean area of surface divergence in **f**. The grey contours represent the bathymetry. **b**–**d**, East–west cross section of temporal averages along 41.65°N for August and September. In **b**, the colours and contours represent the zonal current and potential density anomalies, respectively; 24.0 σ_θ is the density used to determine the layer Froude number (Fr_l). **c**, The colour represents the inverse of the Richardson number (Ri^{-1}). The contour is the region where $Ri^{-1} = 1$. The area enclosed by the magenta line represents the region where Ri^{-1} was averaged for the scatter plot in **e**. The yellow solid line represents Fr_l at each longitude. The bold yellow line represents the region where Fr_l was averaged for the scatterplots in **e** and **f**. **d**, The colours represent the vertical velocity (upward positive), and the contours represent the divergence of the horizontal current. The solid lines indicate positive values (divergence), and the dashed lines indicate negative values (convergence). **e**, and **f**, Scatter plots of region-averaged daily mean Fr_1 and Ri^{-1} and Fr_1 and the surface divergence within the magenta rectangle in **a**, respectively. Source data are provided as a Source Data file.

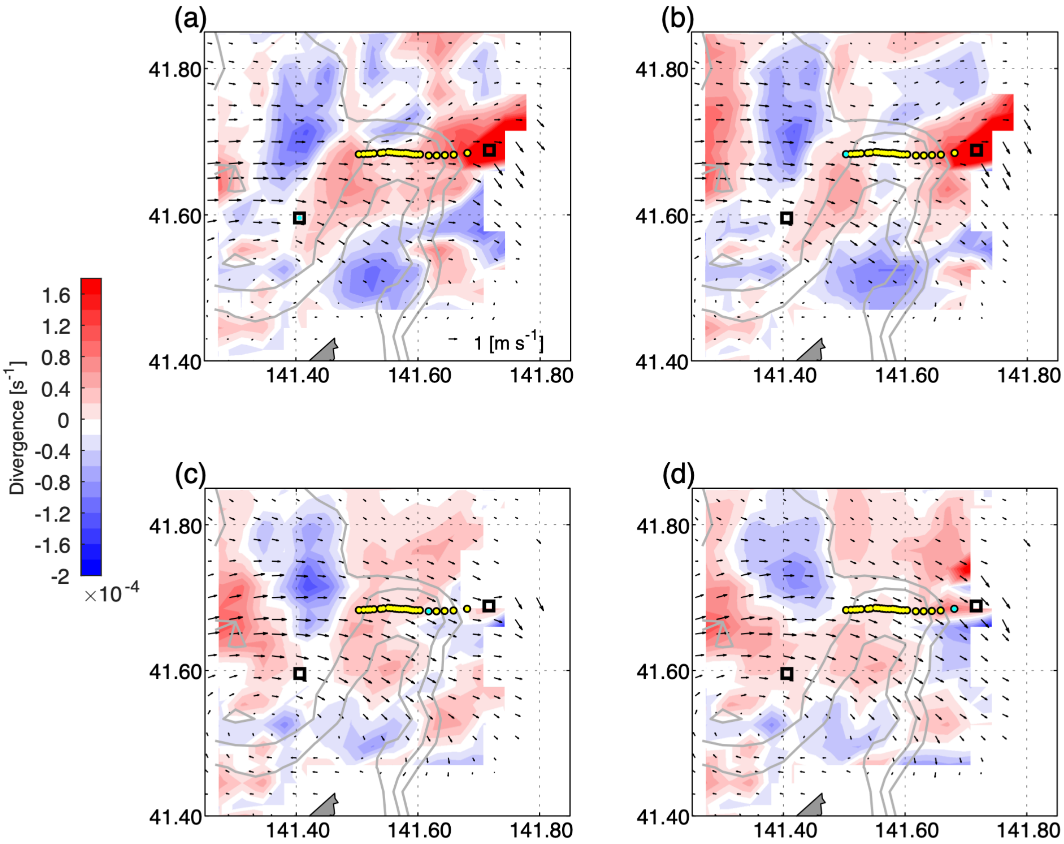

Supplementary Fig. 5 | Divergence of the surface velocity observed by the HFR system on 26th August 2021. The vectors represent the surface velocity observed by the HFR system. **a**, **b**, **c**, and **d** indicate the outputs at 15:00, 16:00, 18:30, and 19:00 (Japan Standard Time), respectively. The yellow dots indicate the deployment points of TurboMAP, and the cyan dots indicate the nearest point of deployment at each time. The squares represent stations where a carousel water sampler was used. The grey contours denote bathymetry. Source data are provided as a Source Data file.

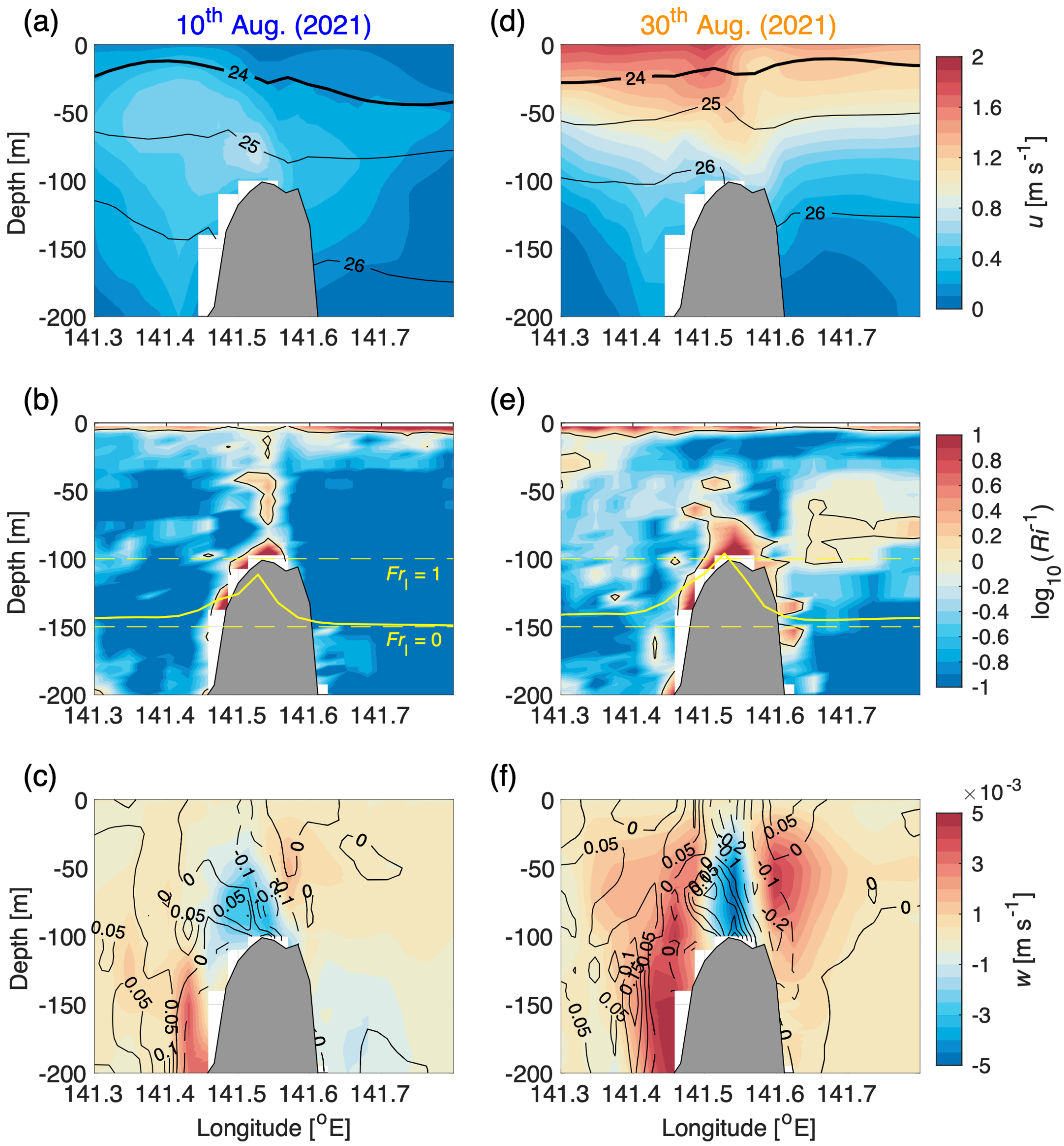

Supplementary Fig. 6 | JCOPE-T DA east–west cross section of the daily mean along 41.65°N on 10th (left column) and 30th (right column) August 2021. a and **d**, Similar to panel **b** in Supplementary Figure 4. **b**, and **e**, similar to panel **c** in Supplementary Figure 4. **c**, and **f**, similar to panel **d** in Supplementary Figure 4. In the case of 10th (30th) August 2021, when the Tsugaru Warm Current flows north (directly above) the Shiriya Spur [see Supplementary Figure 4a], the eastward flow is weak (strong), the Fr_l around the topography is also less (greater) than 1, the region where Ri^{-1} exceeds 1 is also small (large), the upward flow at approximately 141.6°E east of the topography is weak (strong), and the divergence of the surface horizontal velocity east of the spur is also weak (strong). Source data are provided as a Source Data file.

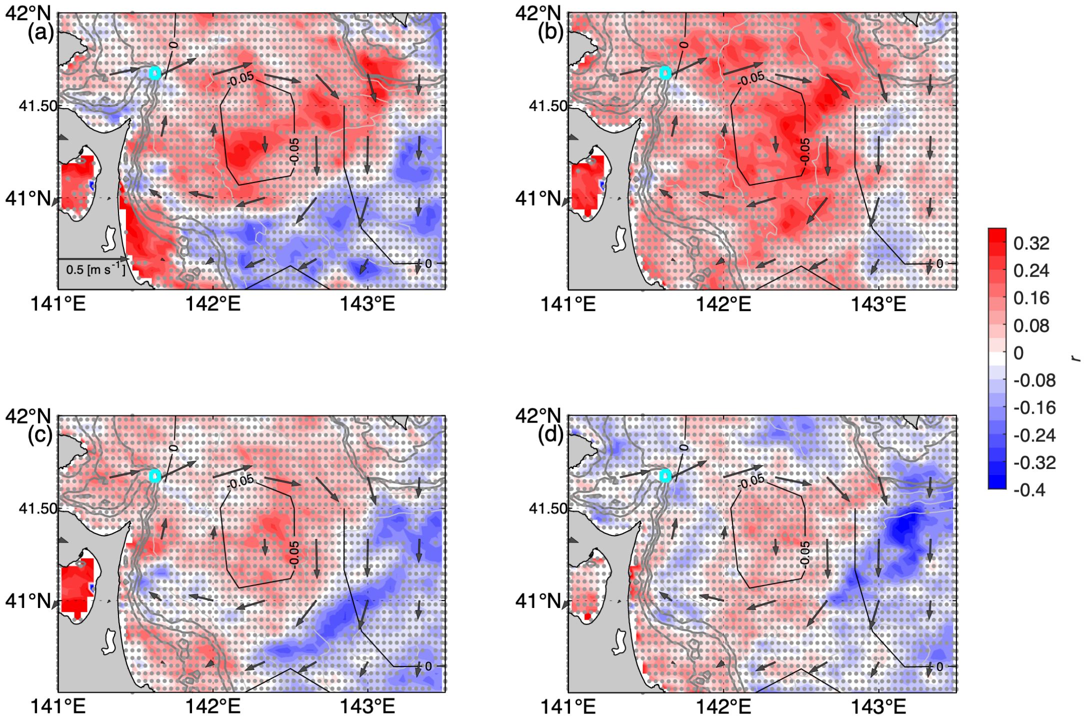

Supplementary Fig. 7 | Lag correlations between surface chlorophyll-*a* and the divergence of surface current velocity on the eastern side of the Shiriya Spur (41.65°N–41.70°N, 141.60°E–141.65°E, delineated by the cyan rectangle; i.e., div_{ES}) in August and September for the years 2014 and 2016–2022. Panels **a**, **b**, **c**, and **d** illustrate cases with 0-day, 3-day, 5-day, and 10-day lags, respectively. The grey dots indicate the grids in which the *p* value is greater than 0.05. The grey contours denote bathymetry. The black contours and vectors are the standardized mean relative vorticity by the inertial frequency at 41°N and the velocity at the surface estimated from OSCAR data between August and September for the years 2014–2021, respectively. Source data are provided as a Source Data file.

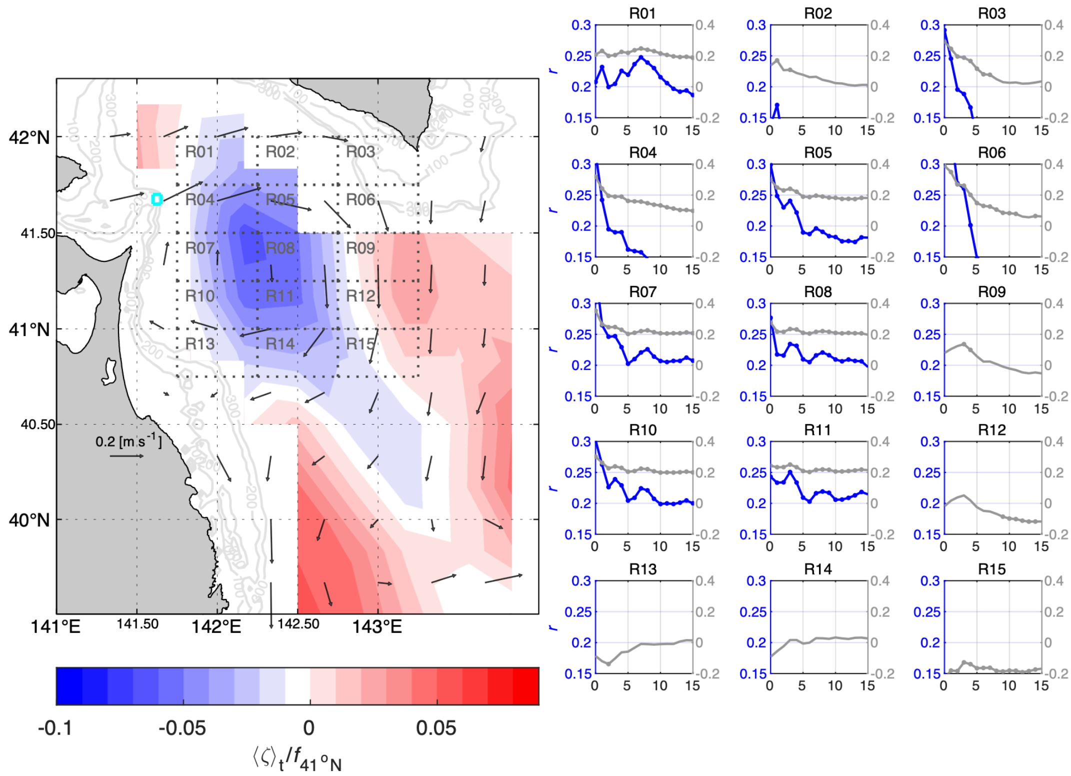

Supplementary Fig. 8 | Lagged correlation analysis between the surface velocity divergence on the eastern flank of the Shiriya Spur derived from the HFR system (*div*$_{\mathrm{ES}}$) and surface chlorophyll-*a* concentrations in August for the years 2014 and 2016–2022. The vector and colour scheme representations in the left panel represent the August mean surface velocity and relative vorticity (normalized to an inertial frequency of 41°N) derived from OSCAR data for 2014–2021. The cyan box delineates the average area for the divergence of surface velocities (*div*$_{\mathrm{ES}}$). The delineated regions on the map (R01–R15) correspond to those shown in the right panels. The blue and grey colours denote the values for the range of the correlation coefficient for 0.15–0.3 (range concentrated display) and −0.2–0.4 (expanded display), respectively. Dots indicate correlation coefficients with p values less than 0.05. In addition to the short timescale lags (~3 days), peaks in significant positive correlation coefficients were observed on timescales exceeding 5 days for R07, R08, R10, and R11. This observation aligns with the notion of an advection effect of recirculation with a timescale of ~3 days, including the second round of recirculation (see Fig. 6 in the main text). Source data are provided as a Source Data file.

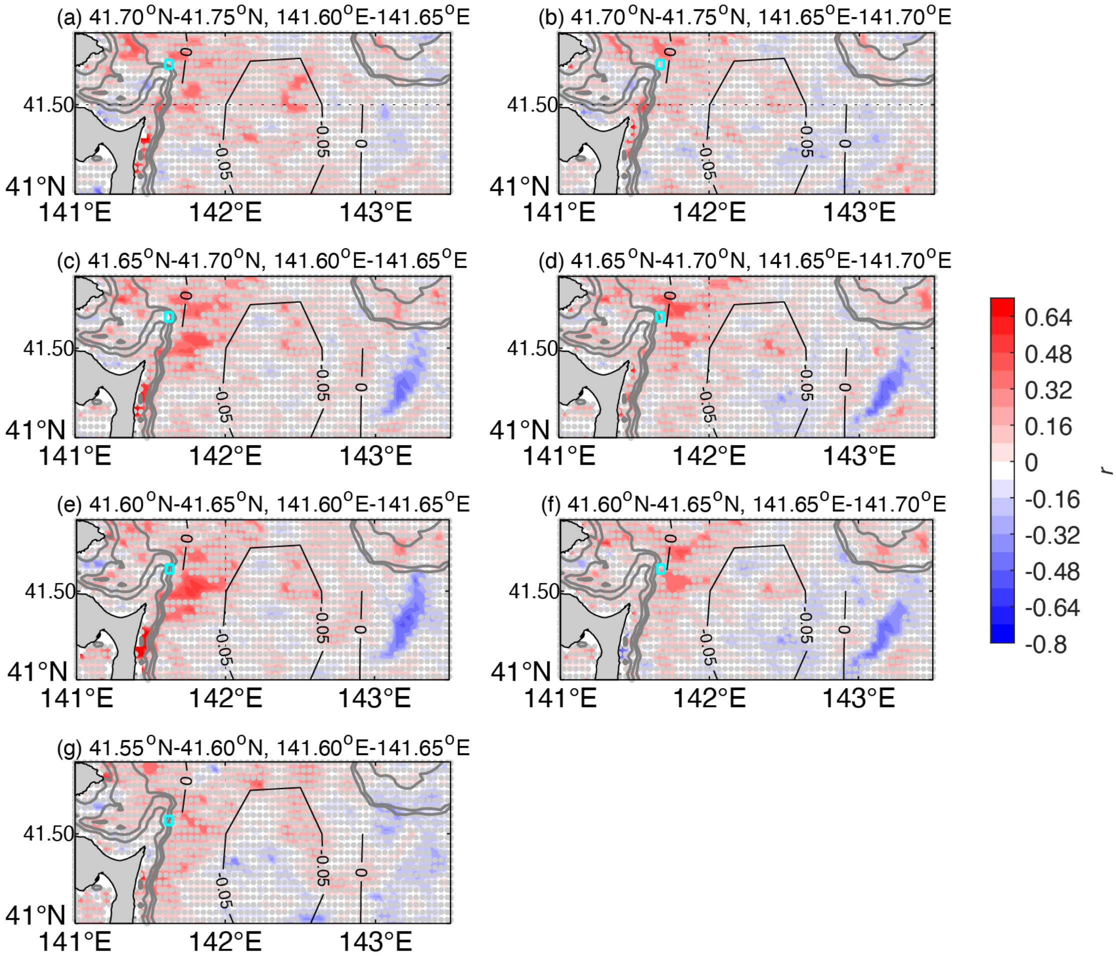

Supplementary Fig. 9 | One-day lag correlation maps between the surface chlorophyll-*a* concentration in the Tsugaru Gyre development season and the divergence of the surface velocity in August and September for the years 2014 and 2016–2022. The area for divergence estimation (div_{ES}) is delineated by the cyan rectangle, which is situated on the eastern side of the Shiriya Spur. The time series were analysed for correlations, excluding the 3-day moving average. The grey dots indicate the grids in which the p value is greater than 0.01. The case of 41.55°N–41.60°N, 141.65°E–141.70°E is excluded because the area is outside the radar measurement range. The black contours are the standardized mean relative vorticity by the inertial frequency at 41°N estimated from OSCAR data between August and September for the years 2014–2021. The grey contours denote bathymetry. Source data are provided as a Source Data file.

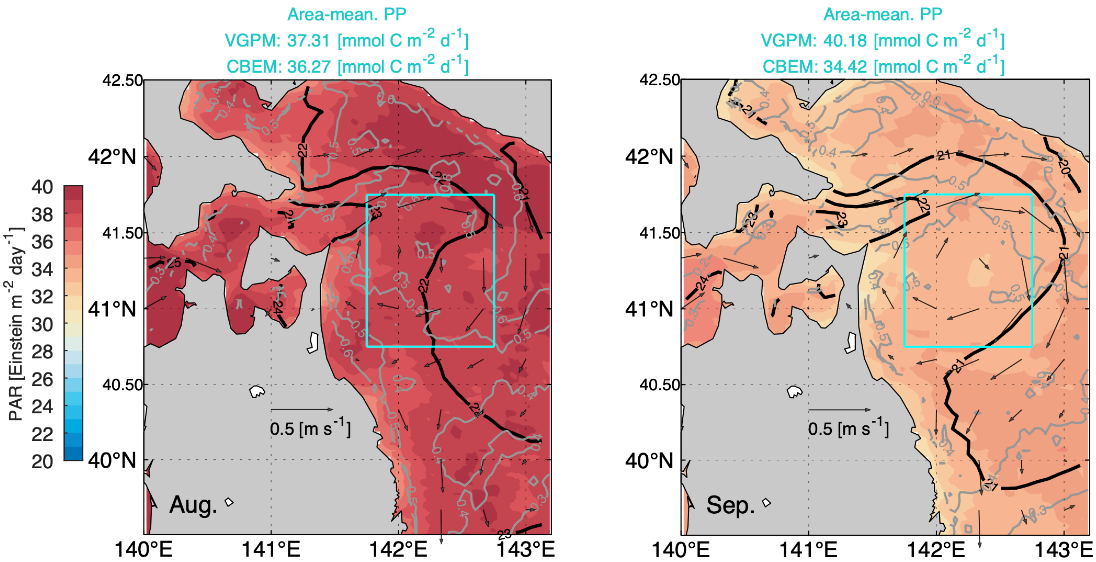

Supplementary Fig. 10 | Monthly means of photosynthetically available radiation (PAR, colours), temperature (black contours), chlorophyll-*a* concentration (grey contours), and Ocean Surface Current Analysis Real-time (OSCAR) velocity (vectors) at the sea surface (2014–2022 except for OSCAR, 2014–2021 for OSCAR). The left and right columns correspond to August and September, respectively. The cyan rectangle delineates the region for the estimation of the mean vertically integrated primary production (PP). Estimates from the vertical generalized production model (VGPM) and the surface chlorophyll-based empirical model (CBEM) are indicated. Source data are provided as a Source Data file.

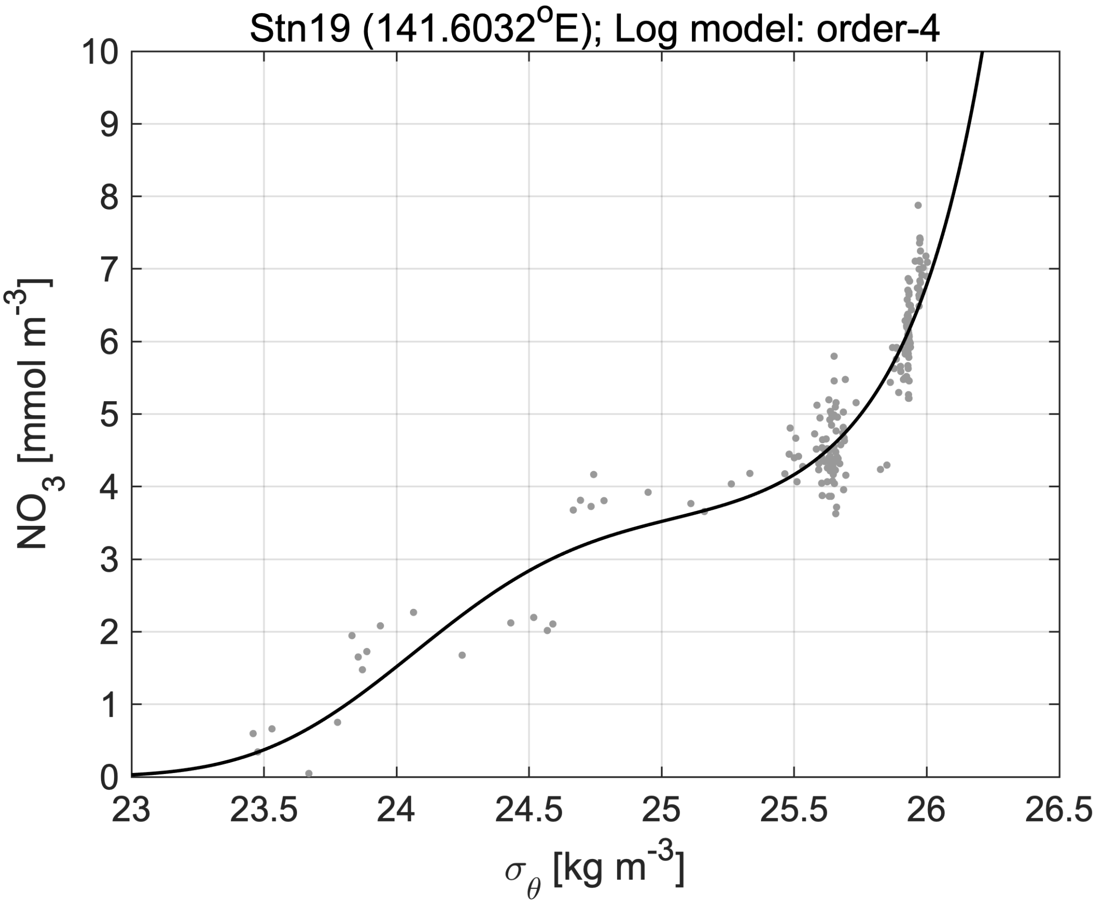

Supplementary Fig. 11 | An example of a multiple linear regression model between density and nitrate concentration. Station 19 at 141.6032°E along the drift line is indicated.

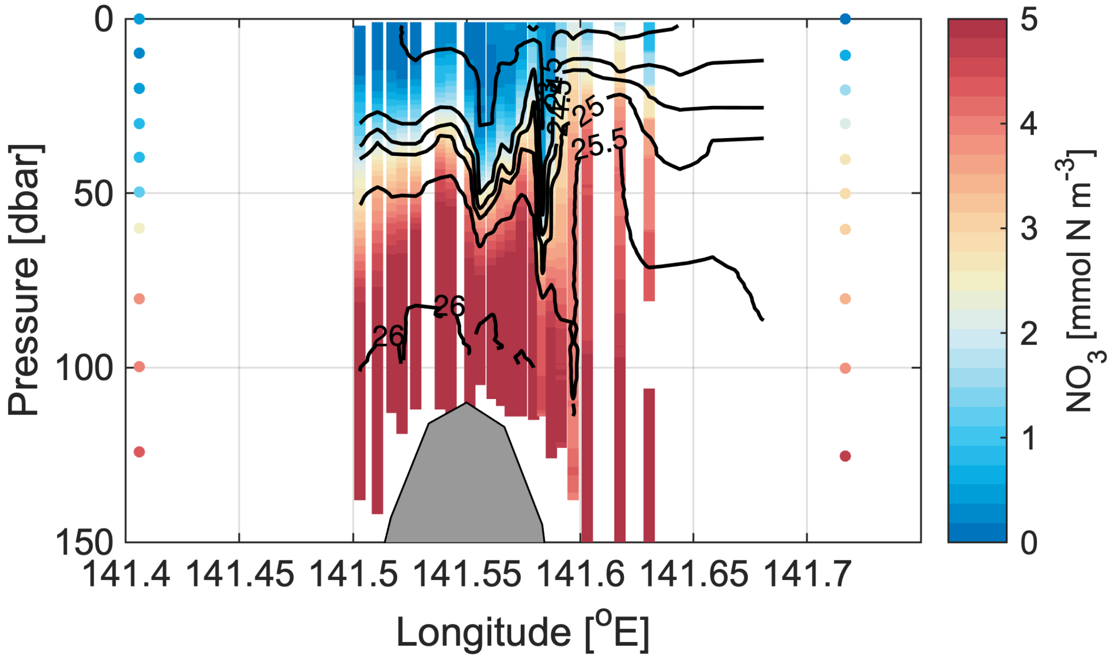

Supplementary Fig. 12 | Vertical transects of nitrate along the drift. The thick black contours denote potential density anomalies. The circular markers denote the data gathered by the carousel water sampler at both the commencement (41.60°N, 141.41°E) and culmination (and 41.69°N, 141.72°E) of the drift observation. Source data are provided as a Source Data file.

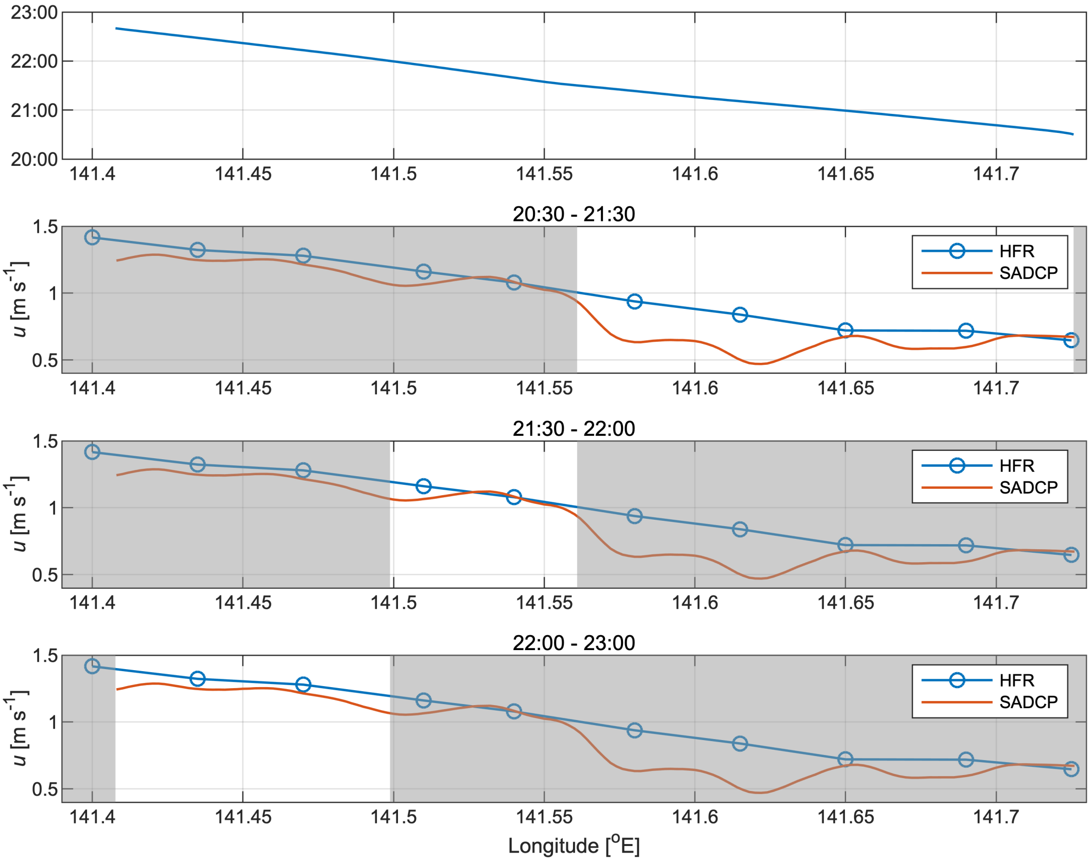

Supplementary Fig. 13 | Comparison of zonal velocity between that estimated from the HFR system and that obtained from the SADCP. Source data are provided as a Source Data file.

Supplementary Table 1 | TurboMAP deployment latitude, longitude, and time

Station No.	Latitude [°N]	Longitude [°E]	Deployment start time (Japan Standard Time) date: 26th Aug. 2021	Surface water sampling	Remarks
Stn. 01	41.683	141.503	16:09	o	
Stn. 02	41.683	141.511	16:14	o	
Stn. 03	41.683	141.517	16:20	o	
Stn. 04	41.684	141.522	16:25	o	
Stn. 05	41.684	141.528	16:30	o	
Stn. 06	41.685	141.538	16:41	o	
Stn. 07	41.685	141.543	16:45	o	
Stn. 08	41.686	141.551	16:53	o	
Stn. 09	41.686	141.556	16:58	o	
Stn. 10	41.685	141.561	17:04	o	
Stn. 11	41.685	141.565	17:09	o	
Stn. 12	41.684	141.569	17:13		
Stn. 13	41.684	141.574	17:18	o	
Stn. 14	41.685	141.580	17:24		
Stn. 15	41.684	141.583	17:28	o	
Stn. 16	41.683	141.587	17:33		
Stn. 17	41.683	141.592	17:39	o	
Stn. 18	41.683	141.597	17:44		
Stn. 19	41.683	141.603	17:50	o	
Stn. 20	41.681	141.618	18:03		
Stn. 21	41.681	141.630	18:17	o	
Stn. 22	41.682	141.644	18:32		SUNA low battery
Stn. 23	41.682	141.658	18:47	o	SUNA low battery
Stn. 24	41.685	141.681	19:04		SUNA low battery

Supplementary Table 2 | Monthly mean sunshine duration at onshore stations surrounding the Tsugaru Gyre (see Fig. 1e for their locations)

	Mutsu	Odanosawa	Hakodate	Kakkumi	Muroran	Tomakomai	Shizunai	Urakawa	Erimo	Statistical Mean
Lon. [ºN]	41.28	41.24	41.82	41.91	42.31	42.62	42.34	42.16	41.93	
Lat. [ºE]	141.21	141.40	140.75	140.97	140.98	141.55	142.36	142.78	143.24	
Duration	1991 –2020	1991 –2020	1991 –2020	1991 –2020	1991 –2020	1991 –2020	1991 –2020	1991 –2020	1991 –2020	
N	30	30	30	30	30	30	30	30	30	
	sunshine duration [hour]	sunshine duration [hour]	sunshine duration [hour]	sunshine duration [hour]	sunshine duration [hour]	sunshine duration [hour]	sunshine duration [hour]	sunshine duration [hour]	sunshine duration [hour]	sunshine duration [hour]
Jan.	67.7	95.5	103.1	113.0	88.3	142.0	138.5	142.0	159.5	116.6
Feb.	88.2	117.6	117.9	124.0	123.6	144.7	156.2	160.8	175.9	134.3
Mar.	141.3	169.9	158.7	166.5	183.7	165.6	188.9	194.2	208.1	175.2
Apr.	184.7	195.9	186.1	184.7	198.9	173.5	190.1	187.9	196.9	188.7
May	196.9	200.5	198.5	190.6	194.9	171.9	199.9	187.2	183.6	191.6
Jun.	163.6	157.3	172.6	144.5	155.8	119.7	163.0	145.0	139.3	151.2
Jul.	131.5	130.0	134.4	129.7	133.2	108.1	128.2	115.6	123.0	126.0
Aug.	139.0	145.2	148.0	135.5	144.9	122.2	144.7	136.0	127.8	138.1
Sep.	145.0	153.4	160.8	153.3	166.5	153.1	152.6	163.4	161.4	156.6
Oct.	150.7	159.4	163.9	158.3	165.2	156.0	156.0	172.2	179.6	162.4
Nov.	98.3	113.0	109.4	118.5	102.7	127.1	116.1	121.7	135.2	115.8
Dec.	70.6	96.3	91.5	99.0	71.1	127.6	113.7	113.2	135.1	102.0

Supplementary Table 3 | Corresponding table of previous literature values for nitrate fluxes and their symbol characteristics in Fig. 2d of the main text.

The subscripts SR and the numbers refer to those given in the Supplementary References.

				mmol N m^{-2} day^{-1} (Bold: Order)				
Authors	Year	Region	Symbols in this paper	mean	±	median	min.	max.
Fernández-Castro et al.[SR1]	2015	Tropical and subtropical Atlantic, Pacific and Indian oceans	T/ST/E	0.171	0.19	-	-	-
Mouriño-Carballido et al.[SR2]	2021	Tropical and subtropical Atlantic and Pacific oceans	T/ST/E	0.4	1	-	-	-
Mouriño-Carballido et al.[SR2]	2021	Tropical and subtropical regions (Literature Summary)	T/ST/E	-	-	0.18	0.00004	8.2
Randelhoff et al.[SR3]	2020	Arctic (Literature Summary)	A	-	-	-	-	-
Mouriño-Carballido et al.[SR2]	2021	Antarctic	AA	102	165	-	-	-
Low et al.[SR4]	2003	Antarctic Circumpolar Current	AA	0.17	-	-	-	0.5 (90%CI)
Doubell et al.[SR5]	2018	Great Australian Bight	Sh/U	-	-	-	**0.0432**	**42.7**
Mouriño-Carballido et al.[SR2]	2021	Shelf seas and upwelling regions (Literature Summary)	Sh/U	-	-	1.7	0.02	300
Tsustumi et al.[SR6]	2020	Kuroshio Region	K	4.7	1.9	-	-	-
Acabado et al.[SR7]	2021	Kuroshio Region	K	-	-	-	0	10
Liu et al.[SR8]	2013	Kuroshio Region	K	-	-	-	0.002	1.542
Kobari et al.[SR9]	2020	Kuroshio Region	K	**1**	-	-	-	-
Tanaka et al.[SR10]	2019	Kuroshio Region	K	-	-	-	**0.01**	**10**
Kaneko et al.[SR11]	2013	Kuroshio Region	K	-	-	-	**0.000864**	**0.0864**
Nagai et al.[SR12]	2021	Kuroshio Region	K	-	-	-	**0.1**	**10**
Hasegawa et al.[SR13]	2021	Kuroshio (Tokara Strait)	K	-	-	-	**1**	**1000**

Supplementary References

1. Fernández-Castro, B. et al. Importance of salt fingering for new nitrogen supply in the oligotrophic ocean. *Nat. Commun.* **6**, 8002 (2015). https://doi.org/10.1038/ncomms9002
2. Mouriño-Carballido, B. et al. Magnitude of nitrate turbulent diffusion in contrasting marine environments. *Sci. Rep.* **11**, 18804 (2021). https://doi.org/10.1038/s41598-021-97731-4.
3. Randelhoff, A. et al. Pan-Arctic Ocean Primary Production Constrained by Turbulent Nitrate Fluxes. *Front. Mar. Sci.* **7**, 150 (2020). https://www.frontiersin.org/articles/10.3389/fmars.2020.00150
4. Law, C. S., Abraham, E. R., Watson, A. J., & Liddicoat, M. I. Vertical eddy diffusion and nutrient supply to the surface mixed layer of the Antarctic Circumpolar Current, *J. Geophys. Res.*, **108** (C8), 3272 (2003). https://doi.org/10.1029/2002JC001604
5. Doubell, M. J., Spencer, D., van Ruth, P. D., Lemckert, C., & Middleton, J. F. Observations of vertical turbulent nitrate flux during summer in the Great Australian Bight. *Deep Sea Res. Part II Top. Stud.* **157–158**, 27–35(2018) . https://doi.org/10.1016/j.dsr2.2018.08.007
6. Tsutsumi, E. et al. Turbulent mixing within the Kuroshio in the Tokara Strait. *J. Geophys. Res. Ocean.* **122**, 7082–7094 (2017). https://doi.org/10.1002/2017JC013049
7. Acabado, C. S., Cheng, Y. H., Chang, M. H., & Chen, C. C. Vertical Nitrate Flux Induced by Kelvin–Helmholtz Billows Over a Seamount in the Kuroshio. *Front. Mar. Sci.* **8**, 680729 (2021). https://doi.org/10.3389/fmars.2021.680729.
8. Liu, X. et al. Variability in nitrogen sources for new production in the vicinity of the shelf edge of the East China Sea in summer. Cont. Shelf Res. **61–62**, 23–30 (2013). https://doi.org/10.1016/j.csr.2013.04.014
9. Kobari, T. et al. Phytoplankton growth and consumption by microzooplankton stimulated by turbulent nitrate flux suggest rapid trophic transfer in the oligotrophic Kuroshio. *Biogeosciences*. **17**, 2441–2452 (2020). https://doi.org/10.5194/bg-17-2441-2020
10. Tanaka, T. et al. Enhanced vertical turbulent nitrate flux in the Kuroshio across the Izu Ridge. *J. Oceanogr.* **75**, 195–203 (2019). https://doi.org/10.1007/s10872-018-

0500-2

11. Kaneko, H., Yasuda, I., Komatsu, K., & Itoh, S. Observations of vertical turbulent nitrate flux across the Kuroshio. *Geophys. Res. Lett.* **40**, 3123–3127 (2013). https://doi.org/10.1002/grl.50613
12. Nagai, T. et al. Elevated turbulent and double‐diffusive nutrient flux in the Kuroshio over the Izu Ridge and in the Kuroshio Extension. *J. Oceanogr.* **77**, 55–74 (2021). https://doi.org/10.1007/s10872-020-00582-2
13. Hasegawa, D. et al. How a small reef in the Kuroshio cultivates the ocean. *Geophys. Res. Lett.* **48**, e2020GL092063 (2021). https://doi.org/10.1029/2020GL092063